*Article*

# Ethylene Glycol Functionalized Gadolinium Oxide Nanoparticles as a Potential Electrochemical Sensing Platform for Hydrazine and p-Nitrophenol

**Savita Chaudhary [1],\*, Sandeep Kumar [1], Sushil Kumar [1] , Ganga Ram Chaudhary [1], S.K. Mehta [1] and Ahmad Umar [2,3],\***

[1] Department of Chemistry and Centre of Advanced Studies in Chemistry, Panjab University, Chandigarh 160014, India; sandeepkumar@gmail.com (S.K.); sushilkumarkai@gmail.com (S.K.); grc22@pu.ac.in (G.R.C.); sav66hooda@gmail.com (S.K.M.)

[2] Department of Chemistry, College of Science and Arts, Najran University, Najran 11001, Saudi Arabia

[3] Promising Centre for Sensors and (Electronic Devices PCSED), Najran University, Najran 11001, Saudi Arabia

\* Correspondence: schaudhary@pu.ac.in (S.C.); umahmad@nu.edu.sa (A.U.); Tel.: +911-722534437 (S.C.); +966-534574597 (A.U.)

check for updates

**Abstract:** The current work reports the successful synthesis of ethylene glycol functionalized gadolinium oxide nanoparticles ($Gd_2O_3$ Nps) as a proficient electrocatalytic material for the detection of hydrazine and p-nitrophenol. A facile hydrothermal approach was used for the controlled growth of $Gd_2O_3$ Nps in the presence of ethylene glycol (EG) as a structure-controlling and hydrophilic coating source. The prepared material was characterized by several techniques in order to examine the structural, morphological, optical, photoluminescence, and sensing properties. The thermal stability, resistance toward corrosion, and decreased tendency toward photobleaching made $Gd_2O_3$ nanoparticles a good candidate for the electrochemical sensing of p-nitrophenol and hydrazine by using cyclic voltammetric (CV) and amperometric methods at a neutral pH range. The modified electrode possesses a linear range of 1 to 10 μM with a low detection limit of 1.527 and 0.704 μM for p-nitrophenol and hydrazine, respectively. The sensitivity, selectivity, repeatability, recyclability, linear range, detection limit, and applicability in real water samples made $Gd_2O_3$ Nps a favorable nanomaterial for the rapid and effectual scrutiny of harmful environmental pollutants.

**Keywords:** gadolinium oxide; hydrazine; p-nitrophenol; electrochemical sensing; amperometric; selective sensor

## 1. Introduction

Aromatic nitro as well as hydrazine are some of the few compounds that are frequently used in the preparation of insecticides, pesticides, pharmaceuticals, and in chemical industries [1–3]. The highly stable nature and lower degradation efficiency of these compounds imparted serious health hazards to human health [4,5]. The utilities of these chemicals in the preparation of explosives are well established in the literature [6]. For instance, according to the U.S Homeland Security Information Bulletin, hydrazine was used in a terrorist attack in 2003 [7]. Hence, from the perspective of safety and security, the development of simple, handy, and competent methodology to monitor these contaminants is the crucial need of the society [8]. To date, there have been a number of analytical instrumental techniques—such as colorimetric, X-ray, fluorescence emission spectroscopy, inductively coupled plasma spectroscopy, atomic absorption spectroscopy, mass spectroscopy, and chromatography—that have been employed for the detection of p-nitrophenol as well as hydrazine [9–12].

All these methods are quite efficient for the detection of these pollutants, but possess delicate functioning, high processing charges, and skilled professionals for data analysis [12]. All these hitches have restricted the use of these sophisticated techniques in routine applications. Hence, from the viewpoint of human health and environmental security, there is a critical requirement for developing alternative techniques with improved selectivity and sensitivity toward these contaminants [13–15]. Therefore, in this work, we have coupled the sensitivity of electrochemical technique with nanoparticles for developing effective sensors for these harmful pollutants. The developed electrochemical sensor has offered significant benefits such as low processing cost and quick response time. The presence of nanoparticles has further augmented the mass transport during analysis as well as reduced the effect of opposition produced by solution during the measurements. The signal-to-noise ratio is further enhanced in the presence of nanoparticles as compared to conventional macroelectrodes used during the analysis. The higher available surface area of nanoparticles has made them an efficient adsorbent for analytes and provided better-quality responses for contaminants.

In the past, varieties of nanoparticles have been used for preparing electrochemical sensors for hydrazine and aromatic compounds [15–20]. For instance, Mishra et al. [15,16] developed the flexible epidermal tattoo, textile and glove-based electrochemical sensor for the detection of organophosphate molecules. The developed sensor was found to be effective in defense and food security applications. Wei et al. [17] have used the nanohybrids of carbon nanotubes (CNTs) with pyrene-cyclodextrin for the electrochemical sensing of p-nitrophenol with sensitivity of around 18.7 $\mu$A/$\mu$M. Karthik et al. [18] have used the applications of gold nanoparticles derived from biogenic sources for sensing hydrazine from aqueous media. The developed sensor has shown a linear range 5 nM to 272 $\mu$M with a detection limit of around 0.05 $\mu$M. Zhang and co-workers have used the application of modified graphene with Pt–Pd nanocubes for detecting aromatic nitro compounds with a detection range of 0.01 to 3 ppm and sensing limit of around 0.8 ppb [19]. Chen et al. [20] have developed the indium tin oxide electrodes, which were further functionalized with $\beta$-cyclodextrin and Ag nanoparticles for analyzing the trace amount of nitroaromatic compounds via using electrochemical sensing analysis. Chaudhary et al. [21] have utilized the fluorescence sensing abilities of $Gd_2O_3$ Nps nanoparticles in the selective detection of 4-nitrophenol in aqueous media. However, the use of $Gd_2O_3$ Nps for the modification of electrodes was less frequent in the literature for the estimation of harmful hydrazine and aromatic compounds.

The current work has utilized the electron transport abilities, high electrical conductivity, and thermal stabilities of $Gd_2O_3$ Nps for making effective material in electrochemical sensing for harmful pollutants [21–23]. To date, a diverse range of methodologies has been investigated for the preparation of $Gd_2O_3$ Nps [24–28]. The available methods have generally required very high temperature reaction conditions and multistep processing for the synthesis of $Gd_2O_3$ Nps. Therefore, it is valuable to systematize a synthetic approach for preparing $Gd_2O_3$ Nps at comparatively low temperature in a minimum number of steps, and formed particles will be reliable for developing an effective sensor for harmful pollutants. The present study has emphasized a hydrothermal route for the preparation of $Gd_2O_3$ Nps under mild conditions. The hydrothermal process is the best preference due to its superior competence, economical nature, flexible reaction constraints, and prospective ability for the large-scale production of particles. The used methodology has provided better control over the size and shape of the formed particles. Abdullah et al. [29] have reported the fabrication of well crystalline $Gd_2O_3$ nanostructures by annealing the hydrothermally prepared nanostructures at 1000 °C. The prepared particles were further used for the detection of ethanol. In the current study, the biocompatible coating of ethylene glycol (EG) has provided better control over the agglomeration rate of formed nanoparticles. The presence of EG has a direct influence over the solubility, optical, luminescence, and the morphological characteristics of the prepared nanoparticles. The external template of EG has also modulated the range of non-radiative energy losses in $Gd_2O$ particles.

Here in this work, surface-modified gadolinium oxide ($Gd_2O_3$) nanoparticles have been used as a proficient electrocatalytic material for the detection of hydrazine and p-nitrophenol by using cyclic voltammetric (CV) and chronoampherometric methods at neutral pH range. The consequences of

synthetic parameters such as the concentration of precursors were studied by measuring the optical, photoluminescence, and band-gap variation of the formed particles. The estimation of the sensitivity, selectivity, repeatability, recyclability, linear range, detection limit, and applicability in real water has also been carried out in the current work. The thermal stability, resistance toward corrosion, and decreased tendency toward photobleaching made $Gd_2O_3$ nanoparticles a probable contender for preparing a simple, fast, and economical electrochemical sensor for hydrazine and p-nitrophenol.

## 2. Experimental Details

### 2.1. Materials

$GdCl_3·6H_2O$ (Gadolinium(III) chloride hexahydrate: Sigma Aldrich, Mumbai, India with purity 99%) was used as a starting material for fabricating $Gd_2O_3$ nanoparticles. EG (ethylene glycol: Fluka 98%) and NaOH (sodium hydroxide: Merck 99.9% pure) were used for the synthesis purpose. Hydrazine, p-nitrophenol, benzaldehyde, benzoic acid, benzonitrile, phenol, ethanol, and aniline were procured from Sigma Aldrich, with purity more than 90%. Acetone (BDH, Mumbai, India, 98%) and ethanol (Changshu Yangyuan, Suzhou, China, 99.9%) were used as the washing solvent for obtained nanoparticles. Millipore distilled water was used for the synthesis of nanoparticles.

### 2.2. Synthesis of $Gd_2O_3$ Nanoparticles

The synthesis of $Gd_2O_3$ nanoparticles was done by using the hydrothermal method. In brief, 5 mM of $GdCl_3·6H_2O$ was added to the 5-mL EG solution under stirring at 50 °C solution followed by the addition of 15 mM NaOH. The temperature of the reaction mixture was held constant at 140 °C for the first hour, and then raised to 180 °C for 4 h. The obtained solution was allowed to cool at room temperature. The obtained yellow precipitates of $Gd_2O_3$ nanoparticles were separated out from the reaction media. The obtained precipitates were subjected to calcinations for 3 h at 300 °C. The resulting particles were washed with water, acetone, and ethanol to remove the impurities. The corresponding separation was mainly performed by ultracentrifugation at 9000 rpm. The extracted particles were dried in an oven at 50 °C and further utilized for different analysis. For the optimization of synthetic parameters for the preparation of $Gd_2O_3$ nanoparticles, the respective concentration variations of $GdCl_3·6H_2O$ have been carried out under respective reaction conditions. In the first instance, the concentration of variations of $GdCl_3·6H_2O$ were done from 5 to 25 mM in all the reaction mixtures by keeping the concentration of the NaOH fixed at 0.015 M. A UV-visible spectral scan for each sample was taken from 230 to 400-nm wavelength to detect the optical properties of the formed nanoparticles. The optical band gap (Eg) of as-prepared nanoparticles was calculated as a function of the concentration variations of $GdCl_3·6H_2O$. The respective fluorescence emission spectra were also studied for the concentration variations of $GdCl_3·6H_2O$ from 5 to 25 mM.

### 2.3. Electrode Preparation

The synthesized nanoparticles were further used to fabricate the electrochemical sensor for hydrazine and p-nitrophenol (Scheme 1). In order to form the modified electrode, the gold electrode with a surface area equivalent to 3.14 $mm^2$ was first cleaned with alumina slurry and properly washed with distilled water under sonication. After drying the electrode at room temperature, the surface of the gold electrode was coated with the $Gd_2O_3$ nanoparticles by using butyl carbitol acetate (BCA) as the binding agent. The as-formed electrode was further dried at 60 ± 5 °C for 4–6 h to attain a homogeneous and dried layer of nanoparticles over the surface of electrode. All the electrochemical measurements were carried out on an µAutolab Type-III under neutral pH conditions. In all the analyses, a $Gd_2O_3$ customized gold electrode was acting as a working electrode, Ag/AgCl (sat. KCl) was acting as a reference, and Pt wire was acting as a counter electrode.
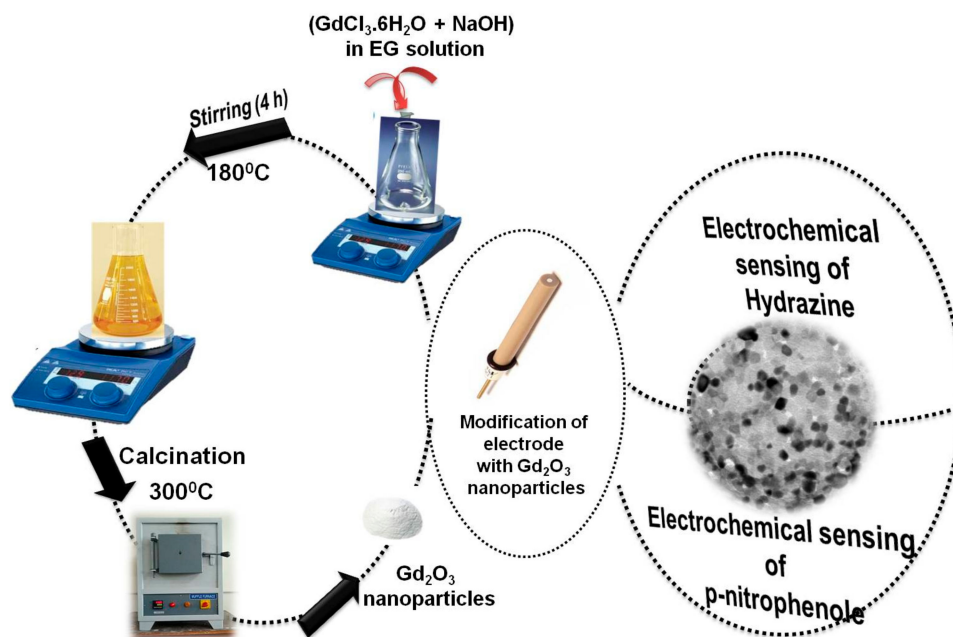
**Scheme 1.** Schematic illustration of the electrochemical sensor for the detection of hydrazine and p-nitrophenol by using the modified electrode of gold with $Gd_2O_3$ nanoparticles.

*2.4. Physical Measurements*

The obtained $Gd_2O_3$ nanoparticles were characterized with the help of an X-ray diffractometer from Panalytical D/Max-2500 (Malvern, UK), Hitachi (H-7500) Transmission electron microscope (Tokyo, Japan), Thermoscientific UV-vis. Spectrophotometer (Waltham, MA, USA), and FTIR spectrophotometer of Perkin-Elmer (RX1) (Waltham, MA, USA). The fluorescence measurements were carried out with a Hitachi F-7000 photoluminescence spectrophotometer. The photoluminescence analysis was carried out on an Edinburgh Instrument FLS 980 (Bain Square, UK). A JEOL (JSM-6610) scanning electron microscope (SEM) (Tokyo, Japan) with EDX analysis was carried out at 20 kV. The calcinations of the as-prepared $Gd_2O_3$ nanoparticles were done in an AICIL muffle furnace at 300 °C. Dynamic light scattering measurements were done on a Malvern Zen1690 instrument (Worcestershire, UK). Raman analysis was performed on a Renishaw inVia reflex micro-Raman spectrometer (Wotton-under-Edge, UK). The pH measurements were performed on a Mettler Toledo digital pH meter (Columbus, OH, USA). The surface area of EG-coated $Gd_2O_3$ nanoparticles was estimated by using Brunauer–Emmett–Teller (BET) analysis with an $N_2$ adsorption analyzer (NOVA 2000e, Anton Par, Gurugram, India). The separation of the as-prepared $Gd_2O_3$ nanoparticles from aqueous media was done on a Remi R-24 centrifuge. Electrochemical measurements were carried out on an μAutolab Type-III cyclic voltammeter (Metrohm, Herisau, Switzerland). The gold electrode with a surface area of 3.14 $mm^2$ was chosen for the analysis.

## 3. Results and Discussion

*3.1. Characterization and Properties of Synthesized $Gd_2O_3$ Nanoparticles*

The crystal structure of formed $Gd_2O_3$ nanoparticles has been further scrutinized by investigating the powdered XRD patterns of formed particles (Figure 1a). The absence of any peak related to impurity has confirmed the purity of the prepared nanoparticles [30]. The average crystallite size (D) of 15 nm has been estimated from the diffraction peaks by using the respective values of full width at half maximum (FWHM) via employing Debye–Scherrer's formula [31,32]. The specific surface area and pore diameter of the obtained sample was found to be 15.3 $m^2 \cdot g^{-1}$ and 2.3 nm, which were respectively calculated by using the nitrogen sorption studies at 77 K in accordance with the BET (Brunauer–Emmett–Teller)

process. The respective atomic content of $Gd_2O_3$ nanoparticles has been confirmed by using EDX analysis (Figure 1b). The obtained spectrum has only displayed the characteristic peaks of the Gd and O atoms in the synthesized sample, which verified the purity of the formed particles.
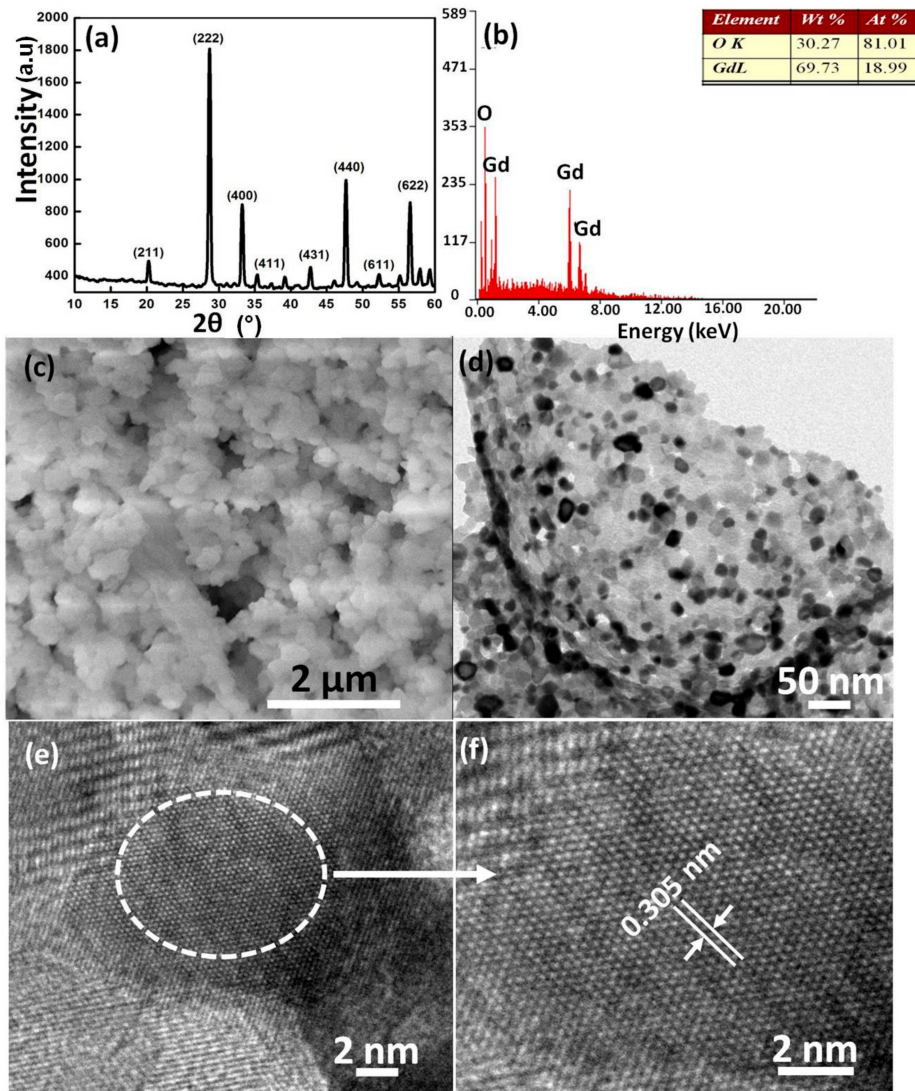


**Figure 1.** Typical (**a**) XRD pattern, (**b**) EDS spectrum, (**c**) SEM image, (**d**) TEM image, and (**e**,**f**) HRTEM images of $Gd_2O_3$ nanoparticles.

The SEM image of the $Gd_2O_3$ nanoparticles has been shown in Figure 1c, which has clearly shown the presence of agglomerated nanostructures of $Gd_2O_3$ nanoparticles. The presence of contacted particles has been mainly due to the existence of an EG template over the surface of the particles, which has further supported the presence of external electrostatic interactive forces generated from the templates over the surface of the nanoparticles. Detailed information regarding the morphology and structure of $Gd_2O_3$ nanoparticles has further been obtained from the HRTEM images presented in Figure 1d. It is clear from the images that the nanoparticles have shown crystallites with an irregular pseudo-spherical shape and a size distribution between 7–15 nm. The crystal spacing of 0.305 nm belongs to the (222) planes of $Gd_2O_3$ nanoparticles (Figure 1e,f). The observed result is in good agreement with the reported literature [33]. The presence of the connected nanocrystals has been attained due to the existence of a diverse range of forces (electrostatic, hydrogen bonding, and van der Waals forces) provided by the presence of external templates of EG coating over $Gd_2O_3$ nanoparticles.

The optical properties of formed $Gd_2O_3$ nanoparticles have been investigated by using UV-vis. and fluorescence analysis as a function of variation of the concentration of $GdCl_3 \cdot 6H_2O$ salt during the synthesis (Figure 2a,b). The formed particles have shown the characteristic peak between 255–262 nm. The respective peak has been associated with the electronic transition from $^8S_{7/2}$–$^6I_{7/2}$. [34]. On interpreting the results, it has been found that the absorbance is dependent on the concentration of salt.
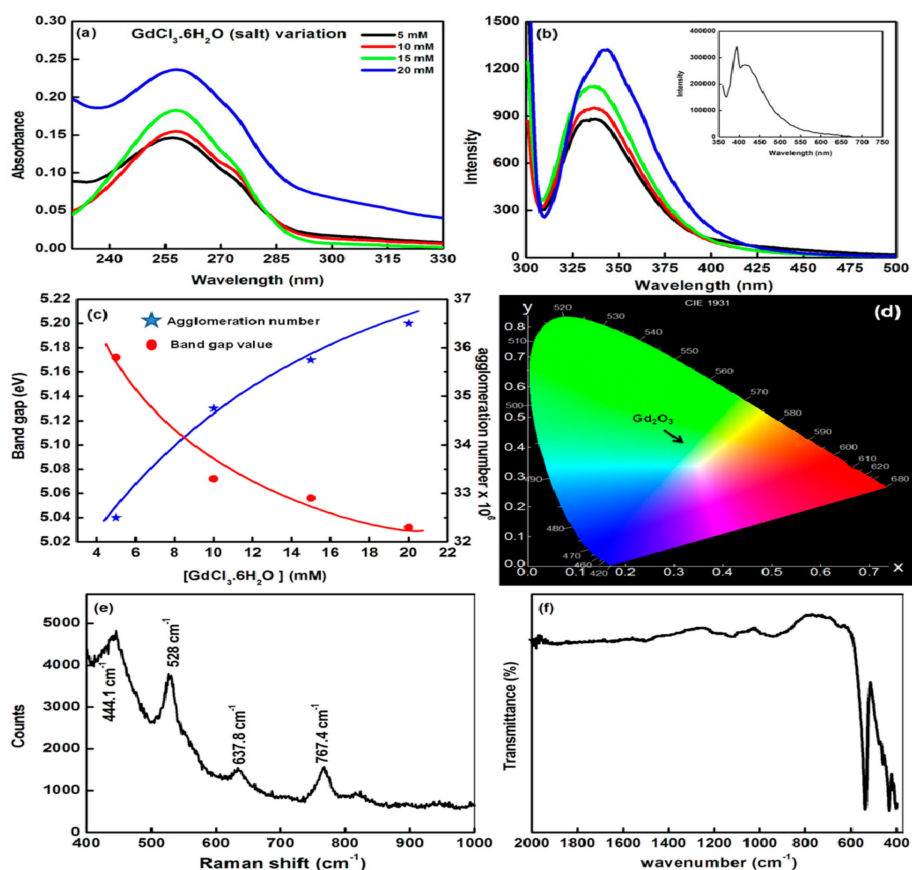


**Figure 2.** (**a**) UV-vis., (**b**) fluorescence and photoluminescence (PL) (inset) emission, (**c**) variation of bandgap and agglomeration number, (**d**) Commission Internationale de L'Eclairage (CIE) chromaticity analysis (**e**) Raman and (**f**) FTIR spectra of $Gd_2O_3$ nanoparticles.

With increase in the concentration from 5 to 20 mM, there has an increment in the absorbance of around 63%. The change in the peak position was not so prominent with the concentration of the salt. On the other hand, a fluorescence emission peak was observed at 336 nm with $\lambda_{exc}$ = 290 nm (Figure 2b). This peak has been associated with the emission from $^6P_{7/2} \leftrightarrow {}^8S_{7/2}$ in Gd(III) ions [35]. The enhancement in the concentration of the starting material has produced an increment of 50.7% in intensity value, whereas the peak position has only shown a change of 10 nm. This variation has displayed the similarity with UV-vis studies. The PL spectra of as-synthesized nanoparticles has shown the characteristic peaks at 390 nm and a broad peak between 400–500 nm with a center at 417 nm ($\lambda_{exc}$ = 350 nm) (inset Figure 2b). The sharp peak at 390 nm has been associated with the radiative recombination of holes with electrons present at the oxygen vacant positions formed due to the photogeneration effect. The other peak was associated with the self-trapped exciton luminescence in formed particles [36]. The optical band-gap values ($E_g$) and agglomeration number for $Gd_2O_3$ nanoparticles (Figure 2c) have been estimated by using the application of the Brus method [37]. The results have clearly explained the behavioral variation of band-gap value with the concentration of $GdCl_3 \cdot 6H_2O$ salt during the synthesis. The decrease in the value of the band gap with the concentration has been associated with the variation of size of the formed particles with the concentration of the

starting material. The particle size was comparatively higher for the nanoparticles prepared with 25 mM $GdCl_3 \cdot 6H_2O$ salt. These variations of starting material have directly influenced the size of the particles, and the respective agglomeration number of the particles has also varied in a similar manner. Figure 2d has displayed the respective assignment of their colors in the Commission Internationale de L'Eclairage (CIE) diagram for the $Gd_2O_3$ nanoparticles. The respective value of CIE chromaticity coordinates is found to be $x = 0.3265$, $y = 0.4462$, respectively. The outcomes have been associated with the green-shift effect in the formed particles. The formed particles have been further characterized by using the Raman and FTIR spectra of $Gd_2O_3$ nanoparticles (Figure 2e,f). On interpretation, $Gd_2O_3$ nanoparticles displayed four major Raman peaks at 444.1, 528, 637.8 and 767.4 $cm^{-1}$, respectively (Figure 2e). These peaks are mainly associated with the Fg and Ag mode for cubic C-type $Gd_2O_3$ particles [38]. Moreover, other Raman active modes such as $4A_g$, $4E_g$, and $14F_g$ have also contributed toward the peaks in the spectra [39,40]. A sharp IR peak has been detected below 500 $cm^{-1}$, which has been attributed to Gd–O [40]. The small peak at 1500 $cm^{-1}$ has been associated with the $\delta$(O–H) vibrations due to the water bound to the nanoparticles surface in the form of moisture [41–44].

### 3.2. Electrochemical Behaviour of Hydrazine and p-Nitrophenol on Modified Electrode

The electrochemical action of formed $Gd_2O_3$ nanoparticles has been investigated toward the electrocatalysis of hydrazine and p-nitrophenol (PNP) via using cyclic voltammetric analysis. Figure 3 showed the cyclic voltammograms of a gold electrode in pH 7.0, phosphate buffer (PBS) under various electrode conditions. Interestingly, it has been found that the bare gold electrode does not show any signal in pH 7 PBS buffer. The response has been still negligible for bulk $Gd_2O_3$-coated gold electrodes in the presence of hydrazine and p-nitrophenol (Figure 3). On the other hand, well-defined voltammetric signals at 0.68 V have been obtained for the electrocatalysis of hydrazine in the presence of a $Gd_2O_3$ nanoparticles-coated gold electrode. In case of p-nitrophenol, one set of reversible redox peaks i.e., $(Gd_{R1})$, oxidation $(Gd_{O1})$ occurred at −0.021 and 0.163 V. Other irreversible reduction peaks $(Gd_{R2})$ at −0.694 V and $(Gd_{R3})$ at 0.4 V were also observed in phosphate buffer solution at pH 7 with a scan rate of 60 mV/s. The obtained results have clearly pointed out that the p-nitrophenol has displayed three types of electrochemical responses with two subsequent types of processes, including reduction and redox couple progression [21]. This might be aroused due to the two-electron oxidation reduction reaction in 4-aminophenol. Whereas, the reduction peaks were associated with the formation of a hydroxylamine group from the nitro group of p-nitrophenol.
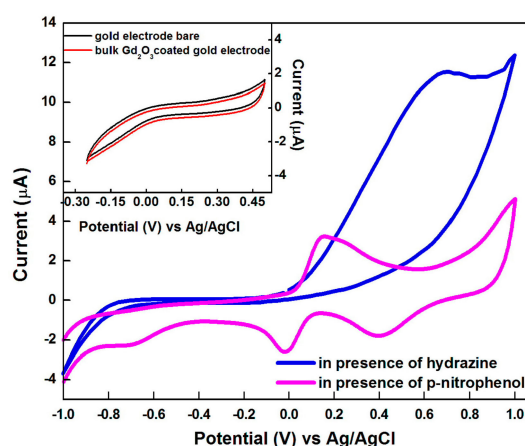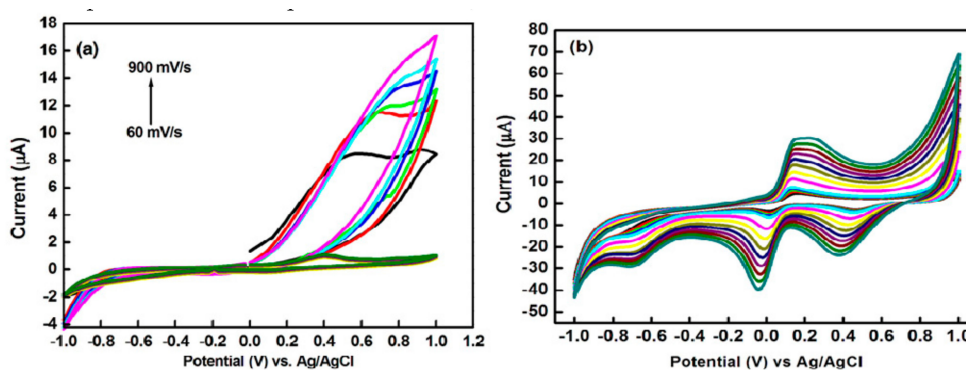


**Figure 3.** Cyclic voltammograms for a $Gd_2O_3$ nanoparticles-coated gold electrode under various electrode conditions in 0.1 M PBS (pH 7.0). The scan rate was 60 mV/s and the respective concentrations of analyte was kept constant at 1 mM.

From Figure 3, it was found that there has been no signal in the reverse sweep for hydrazine samples. The results have confirmed the irreversible nature of the oxidation process for hydrazine.

On other hand, the samples of p-nitrophenol have displayed the redox peaks in both forward and backward directions, which make the analysis of p-nitrophenol reversible in nature [45]. In the presence of $Gd_2O_3$ nanoparticles, there has been found a significant increase in the peak current for respective analytes. This has clearly verified the utilities of formed nanoparticles for electro-analytical purposes. The enhancement of peak current has been mainly explained by the enhancement of conductivity of the electrode due to the functionalization of the gold electrode surface with $Gd_2O_3$ nanoparticles. These results have further validated that the formed $Gd_2O_3$ nanoparticles are capable as efficient electron transporters for the electrocatalysis of harmful pollutants.

The scan rate variations have also been carried out in order to investigate the electron transfer mechanism for a $Gd_2O_3$ modified gold electrode in the presence of hydrazine and p-nitrophenol. Figure 4a,b shows the typical voltammograms for a $Gd_2O_3$ nanoparticles-coated gold electrode with 1 mM solution of respective analyte (i.e., hydrazine and p-nitrophenol) in 0.1 M PBS solution with pH = 7.0 at different scan rates. The spectrum has revealed a regular enhancement of current response with varying the scan rate from 60 to 900 mV/S for both the analytes. The higher surface area of $Gd_2O_3$ nanoparticles has played a critical role for the improved electron transfer process for the catalytic performance toward the understudied analytes. The enhancement of peak current with the scan rate has clearly pointed out the electrocatalytic reaction of hydrazine and p-nitrophenol at the surface of the modified electrode. These current variations have been mainly explained by the surface adsorption to diffusion processes at a façade of modified electrodes [45].



**Figure 4.** Cyclic voltammograms for a $Gd_2O_3$ nanoparticles-coated gold electrode for 1 mM (**a**) hydrazine and (**b**) p-nitrophenol at different scan rates ranging from 60 to 900 mV/s.

At lower scan rates, the relative rate of diffusion is quick, and the adsorption of analyte has been found to be slowest during the mass transfer process. On the other hand, at higher scan rates, the diffusion step has been mainly controlling the rate of electrode reactions in the presence of external agents [46]. In the case of p-nitrophenol, both types of associated processes i.e., the reduction and redox couple processes, have shown the significant augmentation of current response as a function of scan rate. The respective calibration curve of peak current versus the square root of the scan rate has displayed a linear relation for hydrazine and p-nitrophenol (Figure 5). These obtained results have clearly pointed out that the oxidation of hydrazine is mainly a diffusion-controlled process at the surface of a $Gd_2O_3$ nanoparticles-modified gold electrode [47].
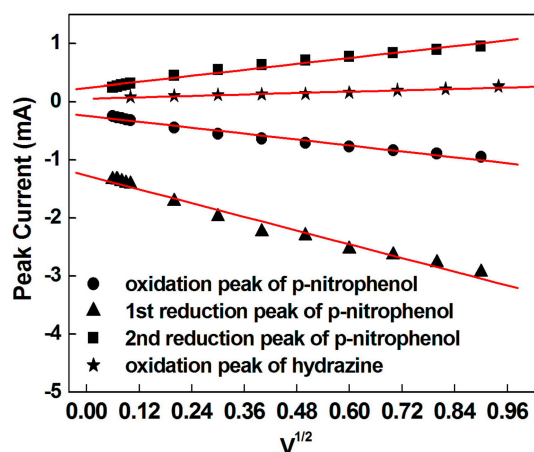
**Figure 5.** The linear dependence of peak current versus square root of scan rate for 1 mM hydrazine and p-nitrophenol.

The number of electrons involved in the overall reaction (*n*) for hydrazine and p-nitrophenol has been calculated from the Randles–Sevcik equation mentioned below [45].

$$ip = \left(2.69 \times 10^5\right)n^{\frac{3}{2}}AD^{\frac{1}{2}}v^{\frac{1}{2}}C \tag{1}$$

where *n* is the number of electron equivalents exchanged during the redox process, $A$ (cm$^2$) is the active area of the working electrode, $D$ (cm$^2 \cdot$s$^{-1}$) and $C$ (mol$\cdot$cm$^{-3}$) are the diffusion coefficient and the bulk concentration of hydrazine, and $v$ is the voltage scan rate (V$\cdot$s$^{-1}$). The obtained CV responses of Gd$_2$O$_3$/Au have clearly explained that the oxidation of N$_2$H$_4$ involves two electron changes, and the irreversible reaction of p-nitrophenol has undergone four electron changes, while the reversible reaction involves two processes—an electron redox process and an irreversible process—and gives a large reduction peak. (Figure 4b) shows the reduction of PNP to 4-(hydroxyamino) phenol. Two coupled redox peaks have indicated the oxidation of 4-(hydroxyamino) phenol to 4-nitrosophenol and the succeeding reversible reduction [48–51]. A schematic representation of the involved mechanism has been illustrated in Scheme 2.
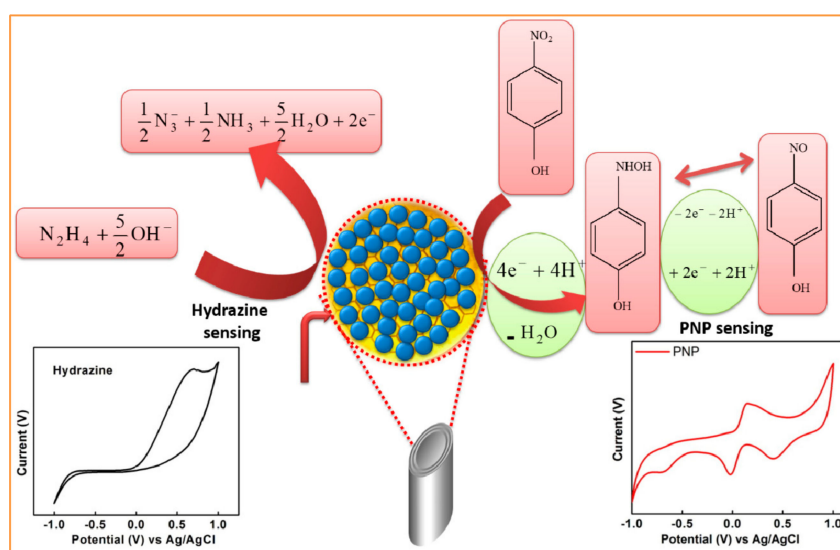


**Scheme 2.** The pictorial representation and cyclic voltammetric sweep curves for the Gd$_2$O$_3$ nanoparticles/butyl carbitol acetate/gold (NPs/BCA/Au) electrode for the sensing of hydrazine and p-nitrophenol.

### 3.3. Amperometric Responses for Hydrazine and p-Nitrophenol

The amperometric studies are one of the primary techniques to estimate the low concentration of analytes and carry out the relative studies in the presence of interfering analytes. Since the $Gd_2O_3$@Au-modified electrode has displayed the higher current response for hydrazine and p-nitrophenol as a model system in the cyclic voltammetric studies, therefore, it has been employed as the amperometric sensor for the detection of hydrazine and p-nitrophenol at low concentration levels.

Figures 6 and 7 depict the amperometric response of $Gd_2O_3$@Au for the successive additions of hydrazine and p-nitrophenol at an applied potential of −0.694 and 0.640 V for p-nitrophenol and hydrazine, respectively, in 0.1 M buffer solution with pH = 7. The obtained values of the current response have been estimated after the consecutive injection of 1 μM concentration of hydrazine and p-nitrophenol at the time interval of 60 s in a continuously stirring condition. The $Gd_2O_3$@Au-modified electrode has exhibited a considerable and rapid amperometric reaction toward each addition of analyte.



(**a**)  (**b**)
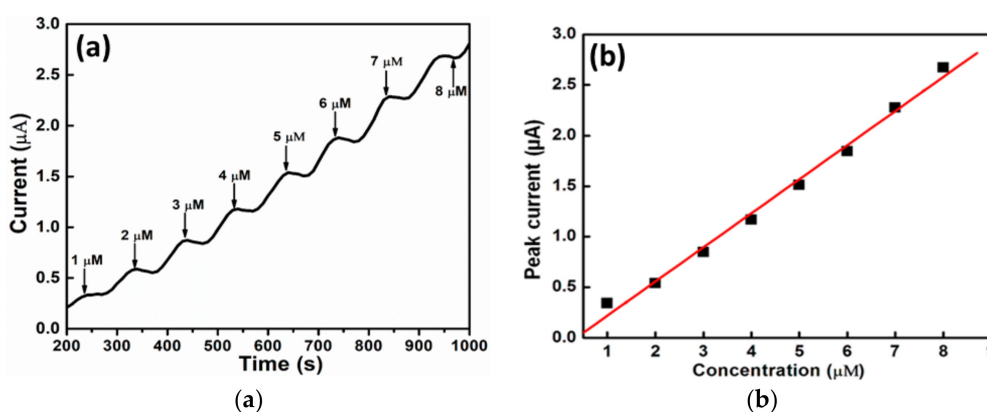
**Figure 6.** (**a**) Amperometric response of the $Gd_2O_3$/Au electrode with an increase in the concentration of hydrazine and (**b**) respective peak current vs. concentration plot of hydrazine in PBS at pH = 7.
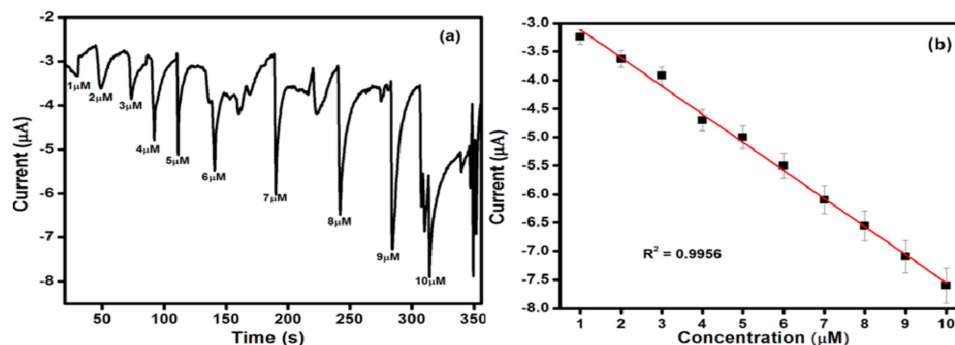


**Figure 7.** (**a**) Amperometric response of the $Gd_2O_3$/Au electrode with an increase in the concentration of p-nitrophenol and (**b**) respective peak current vs. concentration plot of p-nitrophenol in PBS at pH = 7.

The value of the current has reached its stable position within 3 s, demonstrating the fast electro-oxidation of the understudied analyte at the surface of the $Gd_2O_3$@Au-modified electrode. In addition, the response current has shown a linear increment for the subsequent additions of analyte over the wide range of concentrations. The respective regression plot of current response versus concentration of both the analytes has displayed a linear relation with the correlation coefficient values of 0.987 and 0.996 for p-nitrophenol and hydrazine, respectively (Figures 6b and 7b). The limit of detection value has been calculated to be 1.527 and 0.704 μM for p-nitrophenol and hydrazine, respectively, by using the equation limit of detection (LOD) = 3σ/slope, where σ is the standard deviation for the particular system [52]. The sensitivity of the developed sensor has been found to be 0.33722 and 0.25734 mA·mM$^{-1}$ from the slope of the linear regression for hydrazine and p-nitrophenol,

respectively. The respective reusability, stability, and reproducibility of the as-prepared sensor has also been tested in the current work. The as-developed electrode was kept in the buffer media for one month, and its electrocatalytic efficiency has also been tested against the p-nitrophenol and hydrazine. The results have clearly verified that the formed sensor has displayed a reproducible performance with a decay rate of 5.7% and 6.3% in the oxidation peak current value for p-nitrophenol and hydrazine, respectively. This substantial constancy in results has been further attributed to the stability of $Gd_2O_3$ particles, which maintain the efficiency and performance of the electrode for a long period. Additionally, the reproducibility of the developed sensor has been confirmed by estimating the electrochemical response of the $Gd_2O_3$ particles as a working electrode for different electrodes in the solution media containing 1 mM of p-nitrophenol and hydrazine.

The obtained relative standard deviation (RSD) of peak currents has been found to be 5.3% and 4.7%, signifying the satisfactory report for the reproducibility of the modified electrode. In order to investigate the reusability of the developed sensor, the as-modified electrode has been rinsed with the respective sample solution. The obtained signal has been tested after the rinsing. It has been found that the obtained signal has maintained 94% of its original strength. The analytical performance of the as-modified electrode has been evaluated with some recent works in Table 1.

**Table 1.** Comparison of detection limit and response time of different electrode materials.

| Electrode Materials | Analyte | Detection Limit/μM | Response Time/s | Refs. |
|---|---|---|---|---|
| Copper tetraphenylporphyrin (CuTPP) onto zeolites cavity-modified carbon paste electrode | Hydrazine, p-nitrophenol | 1 | – | [53] |
| Multi wall carbon nanotubes (MWCNT) and chlorogenic acid | Hydrazine | 8 | – | [54] |
| Single wall carbon nanotube (SWCNT) and catechin hydrate | Hydrazine and hydroxyl amine | 2.0 | – | [54] |
| Nickel hexacyanoferrate modified carbon ceramic electrode | Hydrazine | 2.28 | <3 | [55] |
| Carbon nanotubes powder microelectrode | Hydrazine | – | <3 | [56] |
| ZnO nanorods | Hydrazine, p-nitrophenol | 2.2 | <10 | [57] |
| $Gd_2O_3$ nanoparticles | – | 0.704 | <10 | This work |

The data has further confirmed the authenticity of the developed sensor in a different range of concentrations with greater selectivity and sensitivity. In order to investigate the application of the formed sensor in real samples, the water samples from different sources have been taken, and the respective analyses have been made for the detection of hydrazine and p-nitrophenol. The relevant stock solutions of understudied analytes of known concentrations were made by using the water samples taken from different sources. The current response of the sensor has been examined for the different concentrations of hydrazine and p-nitrophenol by using amperometric studies. The outcomes of the measurements have shown the excellent recovery rate for the chosen analytes, as indicated in Table 2.

The sensitivity, selectivity, repeatability, recyclability, wide linear range, detection limit, and applicability in real water samples makes $Gd_2O_3$ Nps a favorable nanomaterial in the institution of the rapid and effectual scrutiny of harmful environmental pollutants. Thus, the prepared sensor appears to be a probable contender for preparing a simple, fast, and economical electrochemical sensor.

**Table 2.** Determination of hydrazine and p-nitrophenol real water samples. RSD: relative standard deviation.

| Sample | Added Amount (μM) | Hydrazine | p-Nitrophenol |
|---|---|---|---|
| | | Recovery Mean ± RSD (%) | |
| Tap water | 1.5 | 98.2 ± 2.9 | 97.6 ± 2.5 |
| | 3.5 | 100.2 ± 1.8 | 99.7 ± 3.9 |
| | 7.5 | 101.9 ± 1.5 | 100.3 ± 3.7 |
| Lake water | 1.5 | 96.6 ± 1.5 | 97.3 ± 1.1 |
| | 3.5 | 96.9 ± 2.6 | 99.1 ± 2.4 |
| | 7.5 | 98.4 ± 3.5 | 100.1 ± 1.6 |
| Water from Village Dhanas | 1.5 | 99.6 ± 2.3 | 97.4 ± 1.3 |
| | 3.5 | 100.2 ± 1.4 | 99.4 ± 2.8 |
| | 7.5 | 101.5 ± 1.2 | 100.2 ± 1.2 |

### 3.4. Selectivity Study

In order to apply the proposed sensor for the determination of p-nitrophenol and hydrazine in an aqueous system, the respective selectivity of the sensor has been investigated in the presence of 1 mM of various interfering compounds (benzaldehyde, benzoic acid, benzonitrile, phenol, ethanol, and aniline) at a fixed potential 0.67 V for hydrazine and −0.69 for PNP. Figure 8 has displayed the amperometric response of a $Gd_2O_3$/BCA/Au electrode for the same. From the data, it has been found that a negligible change to response current has been detected in the presence of different interfering compounds. However, significant and quick responses were observed in the presence of hydrazine and PNP. These outcomes have clearly explained the high selectivity of the fabricated sensor toward hydrazine and PNP, and enhanced the scope of the developed sensor.
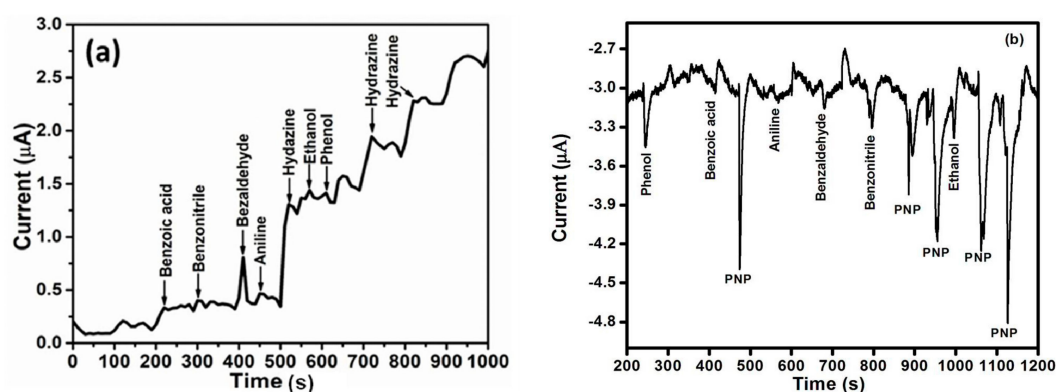


**Figure 8.** Amperometric response of the $Gd_2O_3$/Au electrode in the presence of different analytes with a concentration of 1 mM at pH 7 for (**a**) hydrazine and (**b**) PNP.

## 4. Conclusions

In summary, the current work has reported the fabrication of the ethylene glycol-mediated synthesis of $Gd_2O_3$ Nps. The formation of the particles has been scrutinized by using sophisticated characterization techniques. The effects of synthetic parameters over the optical, photoluminescence, band-gap variation, and agglomeration number of the formed particles have been studied in detail. The fabricated particles have further been employed as a proficient electrocatalytic material for the enzyme-free detection of hydrazine and p-nitrophenol with great sensitivity and selectivity. The developed sensors hold a wider linear range of 1 to 10 μM with low detection limits of 1.527 μM and 0.704 μM for p-nitrophenol and hydrazine, respectively. The sensitivity, selectivity, repeatability, recyclability, wide linear range, and detection limit make $Gd_2O_3$ Nps a favorable nanomaterial in the institution of the rapid and effectual scrutiny of harmful environmental pollutants. The realistic application of the developed sensor has also been investigated by spiking known concentrations of hydrazine and p-nitrophenol in different water samples with good recoveries. Consequently,

the successful synthesis of EG@Gd$_2$O$_3$ nanoparticles has immense potential for the design of highly effective electrochemical sensors, and is a probable way to provide momentum to the advancement of new electrode materials.

## References

1.　Li, J.; Kuang, D.; Feng, Y.; Zhang, F.; Xu, Z.; Liu, M. A graphene oxide-based electrochemical sensor for sensitive determination of 4-nitrophenol. *J. Hazard Mater.* **2012**, *201*, 250–259. [CrossRef] [PubMed]

2.　Nam, G.; Leem, J.-Y. A new technique for growing ZnO nanorods over large surface areas using graphene oxide and their application in ultraviolet sensors. *Sci. Adv. Mater.* **2018**, *10*, 405–409. [CrossRef]

3.　Vernot, E.H.; MacEwen, J.D.; Bruner, R.H.; Haus, C.C.; Kinkead, E.R.; Prentice, D.E.; Hall, A., III; Schmidt, R.E.; Eason, R.L.; Hubbard, G.B.; et al. Long-term inhalation toxicity of hydrazine. *Fundam. Appl. Toxicol.* **1985**, *5*, 1050–1064. [CrossRef]

4.　Savafi, A.; Karimi, M.A. Flow injection chemiluminescence determination of hydrazine by oxidation with chlorinated isocyanurates. *Talanta* **2002**, *58*, 785–792. [CrossRef]

5.　Safavi, A.; Ensafi, A.A. Electrocatalytic oxidation of hydrazine with pyrogallol red as a mediator on glassy carbon electrode. *Anal. Chem. Acta* **1995**, *300*, 307–311. [CrossRef]

6.　Chen, H.; Li, D.; Ding, W. Template-less preparation of meso-MnO$_2$ fibers by localized ostwald ripening and 2,4-dinitrophenol adsorption mechanism. *Sci. Adv. Mater.* **2018**, *10*, 1241–1249. [CrossRef]

7.　U.S. Department of Homeland Security. *Homeland Security Information Bulletin*; U.S. Department of Homeland Security: Washington, DC, USA, 2003.

8.　Shukla, S.; Chaudhary, S.; Umar, A.; Chaudhary, G.R.; Mehta, S.K. Dodecyl ethyl dimethyl ammonium bromide capped WO$_3$ nanoparticles: Efficient scaffolds for chemical sensing and environmental remediation. *Dalton Trans.* **2015**, *44*, 17251–17260. [CrossRef]

9.　Collins, G.E.; Rose-Pehrsson, S.L. Sensitive, fluorescent detection of hydrazine via derivatization with 2,3-naphthalene dicarboxaldehyde. *Analytica Chimica Acta* **1993**, *284*, 207–215. [CrossRef]

10.　Liu, X.; Yang, Z.; Sheng, Q.; Zheng, J. One-pot synthesis of Au-Fe$_3$O$_4$-GO nanocomposites for enhanced electrochemical sensing of hydrazine. *J. Electrochem. Soc.* **2018**, *165*, B596–B602. [CrossRef]

11.　Gao, Y.; Zhang, S.; Hou, W.; Guo, H.; Li, Q.; Dong, D.; Wu, S.; Zhao, S.; Zhang, H. Perylene diimide derivative regulate the antimony sulfide morphology and electrochemical sensing for hydrazine. *Appl. Surf. Sci.* **2019**, *491*, 267–275. [CrossRef]

12.　Guo, W.; Xia, T.; Zhang, H.; Zhao, M.; Wang, L.; Pei, M.A. Molecularly imprinting electrosensor based on the novel nanocomposite for the detection of tryptamine. *Sci. Adv. Mater.* **2018**, *10*, 1805–1812. [CrossRef]

13.　Annalakshmi, M.; Balasubramanian, P.; Chen, S.-M.; Chen, T.-W. One pot synthesis of nanospheres-like trimetallic NiFeCo nanoalloy: A superior electrocatalyst for electrochemical sensing of hydrazine in water bodies. *Sens. Actuators B* **2019**, *296*, 126620. [CrossRef]

14.　Gu, D.; Dong, Y.-M.; Liu, H.; Ding, H.-Y.; Shang, S.-M. Efficient synthesis of highly fluorescence nitrogen doped carbon dots and its application for sensor and cell imaging. *Sci. Adv. Mater.* **2018**, *10*, 964–973. [CrossRef]

15.　Mishra, R.K.; Martin, A.; Nakagawa, T.; Barfidokht, A.; Lu, X.; Sempionatto, J.R.; Lyu, K.M.; Karajic, A.; Musameh, M.M.; Kyratzis, I.L.; et al. Detection of vapor-phase organophosphate threats using wearable conformable integrated epidermal and textile wireless biosensor systems. *Biosens. Bioelectron.* **2018**, *101*, 227–234. [CrossRef] [PubMed]

16.　Mishra, R.K.; Hubble, L.J.; Martin, A.; Kumar, R.; Barfidokht, A.; Kim, J.; Musameh, M.M.; Kyratzis, I.L.; Wang, J. Wearable flexible and stretchable glove biosensor for on-site detection of organophosphorus chemical threats. *ACS Sen.* **2017**, *2*, 553–561. [CrossRef] [PubMed]

17. Wei, Y.; Kong, L.T.; Yang, R.; Wang, L.; Liu, H.; Huang, X.J. Single-walled carbon nanotube/pyrene cyclodextrin nanohybrids for ultrahighly sensitive and selective detection of *p*-nitrophenol. *Langmuir* **2011**, *27*, 10295–10301. [CrossRef]

18. Karthik, R.; Chen, S.M.; Elangovan, A.; Muthukrishnan, P.; Shanmugam, R.; Lou, B.S. Phyto mediated biogenic synthesis of gold nanoparticles using *Cerasus serrulata* and its utility in detecting hydrazine, microbial activity and DFT studies. *J. Colloid Int. Sci.* **2016**, *468*, 163–175. [CrossRef]

19. Zhang, R.; Sun, C.L.; Lu, Y.J.; Chen, W. Graphene nanoribbon-supported Pt-Pd concave nanocubes for electrochemical detection of TNT with high sensitivity and selectivity. *Anal. Chem.* **2015**, *87*, 12262–12269. [CrossRef]

20. Chen, X.; Cheng, X.; Gooding, J.J. Detection of trace nitroaromatic isomers using Indium Tin oxide electrodes modified using β-cyclodextrin and silver nanoparticles. *Anal. Chem.* **2012**, *84*, 8557–8563. [CrossRef]

21. Chaudhary, S.; Kumar, S.; Mehta, S.K. Glycol modified gadolinium oxide nanoparticles as a potential template for selective and sensitive detection of 4-nitrophenol. *J. Mater. Chem. C* **2015**, *3*, 8824–8833. [CrossRef]

22. Du, G.; Tendeloo, G.V. Preparation and structure analysis of $Gd(OH)_3$ nanorods. *Nanotechnology* **2015**, *16*, 595–597. [CrossRef]

23. Mehta, S.K.; Chaudhary, S.; Bhasin, K.K. Understanding the role of hexadecyltrimethylammonium bromide in the preparation of selenium nanoparticles: A spectroscopic approach. *J. Nanopart. Res.* **2009**, *11*, 1759–1766. [CrossRef]

24. Ballem, M.A.; Söderlind, F.; Nordblad, P.; Kall, P.O.; Oden, M. Growth of $Gd_2O_3$ nanoparticles inside mesoporous silica frameworks. *Microporous Mesoporous Mater.* **2013**, *168*, 221–224. [CrossRef]

25. Rahman, A.T.M.; Vasilev, K.; Majewski, P. Ultra small $Gd_2O_3$ nanoparticles: Absorption and emission properties. *J. Colloid Inter. Sci.* **2011**, *354*, 592–596. [CrossRef]

26. Jia, G.; You, H.P.; Liu, K.; Zheng, Y.H.; Guo, N.; Zhang, H.J. Highly uniform $Gd_2O_3$ hollow microspheres: Template-directed synthesis and luminescence properties. *Langmuir* **2010**, *26*, 5122–5128. [CrossRef]

27. Hu, L.; Ma, R.; Ozawa, T.C.; Sasaki, T. Oriented monolayer film of $Gd_2O_3$:0.05Eu crystallites: Quasi-topotactic transformation of the hydroxide film and drastic enhancement of photoluminescence properties. *Angew. Chem. Int. Ed.* **2009**, *48*, 3846–3849. [CrossRef] [PubMed]

28. Manigandan, R.; Giribabu, K.; Suresh, R.; Vijayalakshmi, L.; Stephen, A.; Narayanan, V. Structural, optical and magnetic properties of gadolinium sesquioxide nanobars synthesized via thermal decomposition of gadolinium oxalate. *Mater. Res. Bull.* **2013**, *48*, 4210–4215. [CrossRef]

29. Abdullah, M.M.; Rahman, M.M.; Bouzid, H.; Faisal, M.; Khan, S.B.; Al-Sayari, S.A.; Ismail, A.A. Sensitive and fast response ethanol chemical sensor based on as-grown $Gd_2O_3$ nanostructures. *J. Rare Earths* **2015**, *33*, 214–220. [CrossRef]

30. Chaudhary, S.; Kumar, S.; Umar, A.; Singh, J.; Rawat, M.; Mehta, S.K. Europium-doped gadolinium oxide nanoparticles: A potential photoluminescencent probe for highly selective and sensitive detection of $Fe^{3+}$ and $Cr^{3+}$ ions. *Sens. Actuators B* **2017**, *243*, 579–588. [CrossRef]

31. Mehta, S.K.; Chaudhary, S.; Kumar, S.; Bhasin, K.K.; Torigoe, K.; Sakai, H.; Abe, M. Surfactant assisted synthesis and spectroscopic characterization of selenium nanoparticles in ambient condition. *Nanotechnology* **2008**, *19*, 295601–295612. [CrossRef]

32. Chaudhary, S.; Sharma, P.; Kumar, R.; Mehta, S.K. Nanoscale surface designing of cerium oxide nanoparticles for controlling growth, stability, optical and thermal properties. *Ceram. Int.* **2015**, *41*, 10995–11003. [CrossRef]

33. Maalej, N.M.; Qurashi1, A.; Assadi, A.A.; Maalej, R.; Shaikh, M.N.; Ilyas, M.; Gondal, M.A. Synthesis of $Gd_2O_3$:Eu nanoplatelets for MRI and fluorescence imaging. *Nanoscale Res. Lett.* **2015**, *10*, 215. [CrossRef] [PubMed]

34. Mukherjee, S.; Dasgupta, P.; Jana, P.K. Size-dependent dielectric behaviour of magnetic $Gd_2O_3$ nanocrystals dispersed in a silica matrix. *J. Phys. D Appl. Phys.* **2008**, *41*, 215004–215015. [CrossRef]

35. Rogow, D.L.; Swanson, C.H.; Oliver, A.G.; Oliver, S.R.J. Two related Gadolinium aquo carbonate 2-D and 3-D structures and their thermal, spectroscopic, and paramagnetic properties. *Inorg. Chem.* **2009**, *48*, 1533–1541. [CrossRef] [PubMed]

36. Zhang, Y.; Han, K.; Cheng, T.; Fang, Z. Synthesis, characterization, and photoluminescence property of $LaCO_3OH$ microspheres. *Inorg. Chem.* **2007**, *46*, 4713–4717. [CrossRef] [PubMed]

37. Chaudhary, S.; Umar, A. Glycols functionalized fluorescent $Eu_2O_3$ nanoparticles: Functionalization effect on the structural and optical properties. *J. Alloys Compd.* **2016**, *682*, 160–169. [CrossRef]

38. Rajan, G.; Gopchandran, K.G. Enhanced luminescence from spontaneously ordered $Gd_2O_3$: $Eu^{3+}$ based nanostructures. *Appl. Surf. Sci.* **2009**, *255*, 9112–9123. [CrossRef]

39. White, W.B.; Keramidas, V.G. Vibrational spectra of oxides with the C-type rare earth oxide structure. *Spectrochim. Acta Part A* **1972**, *28*, 501–509. [CrossRef]

40. Riri, M.; Benjjar, A.; Eljaddi, T.; Sefiani, N.; Touaj, K.; Cherif, A.; Hlaïbi, M. Characterization of two dinuclear complexes of the gadolinium ion by IR and Raman. *J. Mater. Environ. Sci.* **2013**, *4*, 961–966.

41. Coats, A.W.; Redfern, J.P. Kinetic parameters from thermogravimetric data. *Nature* **1964**, *201*, 68–69. [CrossRef]

42. Madhusudanan, P.M.; Krishnan, K.; Ninan, K.N. New approximation for the p(x) function in the evaluation of non-isothermal kinetic data. *Thermochimica Acta* **1986**, *97*, 189–201. [CrossRef]

43. Tang, W.; Liu, Y.; Zhang, H.; Wang, Z.; Wang, C. New temperature integral approximate formula for non-isothermal kinetic analysis. *J. Therm. Anal. Calorim.* **2003**, *74*, 309–315. [CrossRef]

44. Horowitz, H.H.; Metzger, G.A. A new analysis of thermogravimetric traces. *Anal. Chem.* **1963**, *35*, 1464–1468. [CrossRef]

45. Singh, K.; Kaur, A.; Umar, A.; Chaudhary, G.R.; Singh, S.; Mehta, S.K. A comparison on the performance of zinc oxide and hematite nanoparticles for highly selective and sensitive detection of para-nitrophenol. *J. Appl. Electrochem.* **2015**, *45*, 253–261. [CrossRef]

46. Raoof, J.B.; Ojani, R.; Beitollahi, H.; Hosseinzadeh, R. Electrocatalytic oxidation and highly selective voltammetric determination of L-cysteine at the surface of a 1-[4-(ferrocenyl ethynyl)phenyl]-1-ethanone modified carbon paste electrode. *Anal. Sci.* **2006**, *22*, 1213–1220. [CrossRef] [PubMed]

47. Shahid, M.M.; Rameshkumar, P.; Basirunc, W.J.; Wijayantha, U.; Chiu, W.S.; Khiew, P.S.; Huang, N.M. An electrochemical sensing platform of cobalt oxide@gold nanocubes interleaved reduced graphene oxide for the selective determination of hydrazine. *Electrochimica Acta* **2018**, *259*, 606–616. [CrossRef]

48. Liu, Z.; Du, J.; Qiu, C.; Huang, L.; Ma, H.; Shen, D.; Ding, Y. Electrochemical sensor for detection of *p*-nitrophenol based on nanoporous gold. *Electrochem. Commun.* **2009**, *11*, 1365–1368. [CrossRef]

49. Ndlovu, T.; Arotiba, O.A.; Krause, R.W.; Mamba, B.B. Electrochemical detection of o-nitrophenol on a poly(propyleneimine)-gold nanocomposite modified glassy carbon electrode. *Int. J. Electrochem. Sci.* **2010**, *5*, 1179–1186.

50. Shukla, S.; Chaudhary, S.; Umar, A.; Chaudhary, G.R.; Mehta, S.K. Tungsten oxide ($WO_3$) nanoparticles as scaffold for the fabrication of hydrazine chemical sensor. *Sens. Actuators B* **2014**, *196*, 231–237. [CrossRef]

51. De Oliveira, F.M.; Guedesa, T.d.; Lima, A.B.; da Silvaa, L.M.; dos Santos, W.T.P. Alternative method to obtain the Tafel plot for simple electrode reactions using batch injection analysis coupled with multiple-pulse amperometric detection. *Electrochimica Acta* **2017**, *242*, 180–186. [CrossRef]

52. Wang, X.; Wang, Q.; Wang, Q.; Gao, F.; Gao, F.; Yang, Y.; Guo, H. Highly dispersible and stable copper terephthalate metal-organic framework-graphene oxide nanocomposite for an electrochemical sensing application. *ACS Appl. Mater. Interfaces* **2014**, *6*, 11573–11580. [CrossRef] [PubMed]

53. Guerra, S.V.; Ubota, L.T.K.; Xavier, C.R.; Nakagaki, S. Experimental optimization of selective hydrazine detection in flow injection analysis using a carbon paste electrode modified with copper porphyrin occluded into zeolite cavity. *Anal. Sci.* **1999**, *15*, 1231–1234. [CrossRef]

54. Salimi, A.; Miranzadeh, L.; Hallaj, R. Amperometric and voltammetric detection of hydrazine using glassy carbon electrodes modified with carbon nanotubes and catechol derivatives. *Talanta* **2008**, *75*, 147–156. [CrossRef] [PubMed]

55. Salami, A.; Abdi, K. Enhancement of the analytical properties and catalytic activity of a nickel hexacyanoferrate modified carbon ceramic electrode prepared by two-step sol–gel technique: Application to amperometric detection of hydrazine and hydroxyl amine. *Talanta* **2004**, *63*, 475–483. [CrossRef]

56. Zhao, Y.D.; Zhang, W.D.; Chen, H.; Luo, Q.M. Anodic oxidation of hydrazine at carbon nanotube powder microelectrode and its detection. *Talanta* **2002**, *58*, 529–534. [CrossRef]

57. Umar, A.; Rahman, M.M.; Hahn, Y.B. ZnO nanorods based hydrazine sensors. *J. Nanosci. Nanotechnol.* **2009**, *9*, 4686–4691. [CrossRef]